INTERNATIONAL JOURNAL OF LATEST TECHNOLOGY IN ENGINEERING, MANAGEMENT & APPLIED SCIENCE (IJLTEMAS)

ISSN 2278-2540 | DOI: 10.51583/IJLTEMAS | Volume XV, Issue VIII, August 2026

Machine Learning Modelling of Geostationary SBAS Satellite Orbit Errors Observed from an Equatorial West African Station

Azeez Ibraheem Abiodun[1]*, Adewumi Adebayo Segun[2], Ayantunji Benjamin Gbenro[3], Sheu Akeem Lawal[1], Ogobor Efua Anthony[3], Eleyele Dolapo Emmanuel[4]

[1]Department of Physics, Emmanuel Alayande University of Education, Oyo, Nigeria

[2]Department of Pure and Applied Physics, Ladoke Akintola University of Technology, Ogbomoso, Nigeria

[3]Physical Science and Life Science Division, National Space Research and Development Agency, Abuja, Nigeria

[4]University of Ilesa, Ilesa, Nigeria

***Corresponding Author**

DOI: https://doi.org/10.51583/IJLTEMAS.2026.150800127

Received: 04 September 2026; Accepted: 09 September 2026; Published: 22 September 2026

ABSTRACT

Geostationary satellites used by satellite-based augmentation systems are continuously visible from equatorial Africa, but their raw broadcast ephemeris accuracy has received limited assessment in West Africa. This study measured and modelled the broadcast orbit errors of three SBAS GEO satellites, comprising EGNOS S23 and S36 and GAGAN S27, observed with a u-blox ZED-F9P receiver at Ogbomoso, Nigeria, from January to March 2026. Broadcast positions were propagated using a second-order Taylor model and compared with interpolated IGS Final precise orbits. Atmospheric drag and piecewise polynomial models were used as mathematical baselines before comparison with Random Forest, XGBoost, support vector regression and long short-term memory models. S23 and S36 maintained stable mean 3D errors near 1.27 m, with standard deviations of approximately 0.55 m. S27 recorded mean errors near 2.6 m in January and February and an isolated March maximum of 97.250 m. The atmospheric drag and polynomial baselines produced RMSE values of 1.329 and 1.293 m, respectively. LSTM achieved 1.282 m, while XGBoost, Random Forest and support vector regression reduced RMSE to 0.272, 0.250 and 0.171 m. The staged residual scheme achieved the lowest RMSE of 0.164 m, representing a 92.8% reduction from the uncorrected value of approximately 2.278 m, and produced a 2DRMS of 1.144 m. The results show that GEO broadcast orbit errors contain nonlinear, satellite-specific patterns that data-driven models can correct effectively, provided anomalous satellites are identified before use.

Keywords: geostationary orbit; SBAS; EGNOS; GAGAN; broadcast ephemeris; orbit error; machine learning; support vector regression; low latitude; Nigeria

INTRODUCTION

Geostationary Earth orbit satellites maintain an approximately fixed position in the sky relative to a ground observer. This provides continuous visibility from stations within their coverage area and gives them a distinct role in satellite navigation. Satellite-based augmentation systems such as the European Geostationary Navigation Overlay Service and the Indian GPS Aided GEO Augmented Navigation system transmit ranging signals and correction information through GEO satellites. The BeiDou Navigation Satellite System also includes GEO satellites as part of its operational constellation (Yang, 2021). For stations near the equator, these satellites generally have high and slowly varying elevation angles, which can provide favourable observing geometry. Their usefulness for ranging, however, also depends on the accuracy and continuity of

ISSN 2278-2540 | DOI: 10.51583/IJLTEMAS | Volume XV, Issue VIII, August 2026

their broadcast ephemerides. GEO broadcast orbit accuracy has received considerably less attention than the corresponding accuracy of medium Earth orbit constellations.

Previous SBAS studies have largely examined the accuracy of the augmentation service rather than the raw GEO broadcast ephemeris. Nie et al. (2019) evaluated five operational SBAS L1 services and reported a signal-in-space range error of 0.645 m for EGNOS, the lowest among the evaluated systems when the transmitted differential corrections were applied. Raw broadcast orbit error is a different quantity because it represents the difference between the satellite position transmitted in the navigation message and a precise reference orbit before augmentation corrections are applied. A review of the available literature found no detailed characterisation of raw GEO broadcast ephemeris errors using observations from a West African monitoring station. This geographical gap matters because correction-message availability, communication latency and service continuity may differ between the centre and edge of an SBAS coverage area. The GEO environment also affects the suitability of conventional orbit-error models. At an altitude of approximately 35,786 km, atmospheric density is extremely low and atmospheric drag has little direct influence on satellite motion. The atmospheric drag model nevertheless provides a physically defined mathematical baseline for testing whether a conventional force-based approach can explain any meaningful part of the observed GEO broadcast error. Its expected limitations at GEO altitude also provide a useful reference for assessing whether model complexity produces a genuine improvement.

A piecewise polynomial model provides a second mathematical baseline. Unlike the atmospheric drag model, it does not assume a specific physical source for the error. Instead, it approximates the locally smooth temporal variation of the observed error within successive time segments. This makes it suitable for capturing gradual changes associated with orbit propagation, ephemeris updates and slowly varying ground-segment effects. However, it may not represent abrupt changes, satellite-specific anomalies or nonlinear relationships between orbit error, observing geometry and temporal variables. Other perturbations are more important at GEO altitude. Lunisolar attraction and solar radiation pressure act over longer timescales and are managed through orbit determination and station-keeping operations (Prange et al., 2020; Pratiwi et al., 2025). Broadcast position accuracy is therefore influenced strongly by the ability of the ground segment to estimate and upload an accurate satellite state vector (Soop, 1994). Consequently, GEO broadcast orbit error may contain less of the smooth dynamically driven structure commonly associated with lower orbital regimes. It may nevertheless contain patterns related to ephemeris update cycles, satellite identity, time and observing geometry. Flexible data-driven models may capture these relationships more effectively than conventional mathematical models. This possibility has not been adequately tested using equatorial West African observations.

This study addresses the gap by analysing three GEO satellites, comprising two EGNOS satellites and one GAGAN satellite, observed for three months from Ogbomoso, Nigeria. Their broadcast positions were compared with IGS Final precise orbit products to determine radial, along-track, cross-track and total three-dimensional orbit errors. The atmospheric drag and piecewise polynomial models were applied as mathematical baselines. Their performance was then compared with Random Forest, XGBoost, support vector regression and long short-term memory models using the same evaluation data. A staged residual correction scheme was subsequently developed to determine whether combining complementary data-driven models could improve upon the individual learners and mathematical baselines. The study provides a characterisation of raw GEO broadcast orbit error from an equatorial West African station and establishes a structured comparison between physical, numerical and data-driven correction methods. It also examines whether locally observed GEO orbit errors can be reduced to the sub-two-decimetre level and assesses how isolated satellite anomalies affect model performance. The findings provide evidence for selecting suitable correction methods and emphasise the need for satellite-specific screening when positioning depends on a small GEO subset.

Data And Study Area

Station, Receiver, and Satellites

The observations were collected at the LAUTECH GNSS Laboratory (LGL), Ladoke Akintola University of Technology, Ogbomoso, Nigeria, at 8.17054400°N, 4.26892783°E, using a u-blox ZED-F9P receiver and

INTERNATIONAL JOURNAL OF LATEST TECHNOLOGY IN ENGINEERING, MANAGEMENT & APPLIED SCIENCE (IJLTEMAS)

ISSN 2278-2540 | DOI: 10.51583/IJLTEMAS | Volume XV, Issue VIII, August 2026

antenna. This low-cost receiver class has been found suitable for precision applications in independent assessments (Adewumi et al., 2025; Hohensinn et al., 2022; Robustelli et al., 2023). Three geostationary satellites were tracked between January and March 2026. The dataset identifies S23 and S36 with EGNOS and S27 with GAGAN. The RINEX identifiers correspond to SBAS PRNs 123, 136 and 127, respectively.

Figure 1. Satellite Image of Observation Location

Raw acquisition was specified at 1 Hz, with five-minute epoch selection in the processing script. Raw UBX files were converted to RINEX 3 using RTKLIB convbin. The resulting analytical record comprised 7,173 satellite epochs for S23, 6,465 for S27 and 7,179 for S36. These counts describe satellite-epoch records and therefore include observations of different satellites at common times. Missing intervals prevent the retained records from being treated as a continuous, uniformly sampled sequence.

METHODS

The complete processing chain, from the raw receiver observations to the corrected positioning solution, is summarised in Figure 2. The atmospheric drag and piecewise polynomial models were implemented as mathematical baselines. Their performance established the level of correction achievable using conventional physical and numerical modelling before comparison with Random Forest, XGBoost, support vector regression, LSTM and the staged residual correction scheme.

Figure 2. Methodological framework adopted for the characterisation and data-driven correction of geostationary SBAS broadcast orbit errors observed at Ogbomoso, Nigeria.

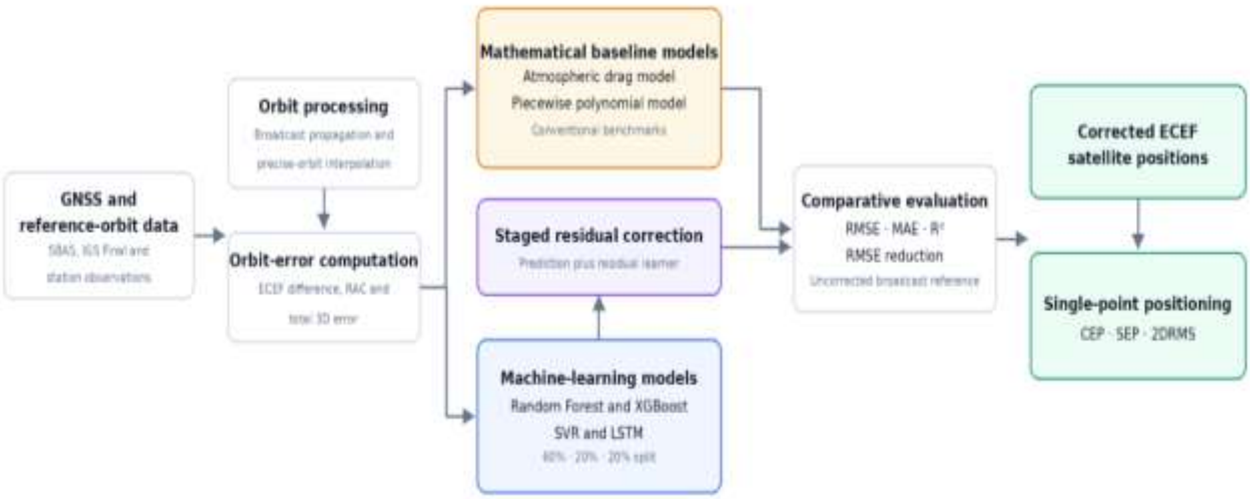

ISSN 2278-2540 | DOI: 10.51583/IJLTEMAS | Volume XV, Issue VIII, August 2026

Broadcast Position Propagation

Each SBAS navigation record supplies an ECEF position, velocity, and acceleration at a reference epoch t_0. The broadcast position at an arbitrary observation epoch t was obtained by second-order Taylor propagation:

$$\mathbf{r}^{\mathrm{bc}}(t) = \mathbf{r}_0 + \mathbf{v}_0\,\Delta t + 1/2\,\mathbf{a}_0\,\Delta t^2, \qquad \Delta t = t - t_0, \quad |\Delta t| \le 90\ \mathrm{s} \qquad (1)$$

where $\mathbf{r}^{\mathrm{bc}}(t)$ is the propagated broadcast position vector, $\mathbf{r}_0$, $\mathbf{v}_0$, and $\mathbf{a}_0$ are the broadcast position, velocity, and acceleration vectors at the reference epoch, and Δt is the propagation interval. The navigation record nearest to each observation epoch was selected.

Reference Orbit Interpolation and Orbit Error Computation

IGS Final positions are tabulated at 15-minute intervals, so each ECEF component was interpolated to the observation epoch with a natural cubic spline:

$$r_c^{\mathrm{pr}}(t) = a_j + b_j(t - t_j) + c_j(t - t_j)^2 + d_j(t - t_j)^3, \quad t \in [t_j, t_{j+1}] \qquad (2)$$

where $r_c^{\mathrm{pr}}(t)$ is the interpolated precise coordinate $c \in \{x, y, z\}$, t_j is the SP3 tabular epoch preceding t, and a_j, b_j, c_j, d_j are the spline coefficients on that interval, fixed by continuity of the function and of its first two derivatives. The orbit error vector was calculated as:

$$\Delta\mathbf{r} = \mathbf{r}^{\mathrm{pr}} - \mathbf{r}^{\mathrm{bc}} \qquad (3)$$

The error vector was subsequently resolved into radial, along-track and cross-track components. The total three-dimensional orbit error was calculated as:

$$\Delta_{3D} = \sqrt{\Delta R^2 + \Delta A^2 + \Delta C^2} \qquad (4)$$

Mathematical Baseline Models

Two conventional models were evaluated as mathematical baselines. These were the atmospheric drag model and the piecewise polynomial model. They provided reference performance against which the machine-learning and staged residual methods were assessed. They were not classified as machine-learning models.

Atmospheric Drag Baseline

The atmospheric drag baseline represented the orbit-error contribution associated with atmospheric resistance:

$$a_D = -\frac{1}{2}\rho C_D \frac{A}{m} \|v_{rel}\| v_{rel} \qquad (5)$$

where ρ\rho is atmospheric density, C_D is the drag coefficient, A/mmiss the satellite area-to-mass ratio and $\boldsymbol{v}_{rel}$ is the satellite velocity relative to the atmosphere. Atmospheric density was obtained using the NRLMSISE-00 model with the $F_{10.7}$ solar-flux and Ap geomagnetic indices.

The drag model was retained as a physical baseline even though atmospheric drag is weak at geostationary altitude. Its inclusion allowed the data-driven models to be compared with a conventional perturbation-based method.

Piecewise Polynomial Baseline

The piecewise polynomial model represented the locally smooth temporal behaviour of the orbit-error components. Within each time segment, an error component $\boldsymbol{q} \in \{\mathrm{R,A,C}\}$ was approximated by:

ISSN 2278-2540 | DOI: 10.51583/IJLTEMAS | Volume XV, Issue VIII, August 2026

$$\widehat{\Delta q(t)} = \sum_{p=0}^{P} \beta_{p,j} \left(t - t_j\right)^p \qquad (6)$$

where P is the polynomial order and $\beta_{p,j}$ represents the coefficient of term p in segment j. The coefficients were estimated using the training observations within each segment. The model was fitted independently to the radial, along-track and cross-track errors.

The polynomial model provided a numerical baseline for assessing whether machine-learning methods could capture error patterns beyond the locally smooth variations represented by conventional polynomial fitting.

Feature Construction and Data Partitioning

Each satellite-epoch record was described using lagged orbit-error components, temporal variables, observing geometry, broadcast state-vector magnitudes and space-weather indices. The target vector contained the radial, along-track and cross-track errors at the current epoch:

$$\mathbf{y}_k = [\Delta R_k, \Delta A_k, \Delta C_k]^{\mathrm{T}} \qquad (7)$$

Continuous predictors were standardised using only the mean and standard deviation of the training subset. The observations were divided chronologically into training, validation and test subsets using proportions of 60%, 20% and 20%, respectively. This chronological division was applied consistently to the mathematical baselines and data-driven models to support a fair comparison and reduce temporal leakage.

Machine Learning Models

Four machine-learning models were evaluated against the atmospheric drag and piecewise polynomial baselines. These were Random Forest, XGBoost, support vector regression and LSTM. The models predicted the current radial, along-track and cross-track orbit-error components from the constructed features.. The random forest averages an ensemble of regression trees grown on bootstrap samples with a random feature subset evaluated at each split,

$$\hat{\mathbf{y}}_k^{\mathrm{RF}} = \frac{1}{B} \sum_{b=1}^{B} T_b\,(\mathbf{x}_k) \qquad (8)$$

where $\hat{\mathbf{y}}_k^{\mathrm{RF}}$ is the ensemble prediction, $B = 200$ is the number of trees, and T_b is the b-th tree.

XGBoost fits shallow trees sequentially in a stagewise additive expansion under a regularised squared-error objective,

$$\hat{y}_k^{(m)} = \hat{y}_k^{(m-1)} + \eta\, f_m(\mathbf{x}_k) \qquad (9)$$

$$\mathcal{L} = \sum_{k} (y_k - \hat{y}_k)^2 + \sum_{m} (\gamma L_m + 1/2\, \lambda \parallel w_m \parallel^2) \qquad (10)$$

where $\hat{y}_k^{(m)}$ is the prediction after m boosting rounds, η is the learning rate, f_m is the tree added at round m, L_m is its number of leaves, w_m is its vector of leaf weights, and γ and λ are the complexity and shrinkage penalties.

Support vector regression fits the flattest function that deviates from each observed target by no more than ϵ,

$$\min_{w,b,\xi,\xi^*} 1/2 \parallel w \parallel^2 + C \sum_{k=1}^{n} (\xi_k + \xi_k^*) \quad \text{subject to} \quad |y_k - f(\mathbf{x}_k)| \le \epsilon + \xi_k^{(*)} \qquad (11)$$

ISSN 2278-2540 | DOI: 10.51583/IJLTEMAS | Volume XV, Issue VIII, August 2026

$$K(\mathbf{x}_k, \mathbf{x}_l) = \exp(-\gamma_K \parallel \mathbf{x}_k - \mathbf{x}_l \parallel^2) \qquad (12)$$

where w is the weight vector in feature space, b is the bias, ξ_k and ξ_k^* are slack variables for deviations above and below the tube, C is the regularisation parameter, ϵ is the tube width, K is the radial basis function kernel, and γ_K is the kernel bandwidth. The parameters C and γ_K were tuned by five-fold cross-validation on the training set.

A long short-term memory (LSTM) network operated on sequences of ten consecutive epochs, with each cell updating according to

$$\mathbf{f}_t = \sigma\big(W_f[\mathbf{h}_{t-1}, \mathbf{x}_t] + b_f\big), \quad \mathbf{i}_t = \sigma(W_i[\mathbf{h}_{t-1}, \mathbf{x}_t] + b_i), \quad \mathbf{o}_t = \sigma(W_o[\mathbf{h}_{t-1}, \mathbf{x}_t] + b_o) \qquad (13)$$

$$\mathbf{c}_t = \mathbf{f}_t \odot \mathbf{c}_{t-1} + \mathbf{i}_t \odot \tanh(W_c[\mathbf{h}_{t-1}, \mathbf{x}_t] + b_c), \qquad \mathbf{h}_t = \mathbf{o}_t \odot \tanh(\mathbf{c}_t) \qquad (14)$$

where $\mathbf{f}_t$, $\mathbf{i}_t$, and $\mathbf{o}_t$ are the forget, input, and output gate activations at step t, $\mathbf{c}_t$ is the cell state, $\mathbf{h}_t$ is the hidden state, $W_\bullet$ and $b_\bullet$ are the corresponding weight matrices and bias vectors, σ is the logistic sigmoid, and $\odot$ denotes elementwise multiplication. The network used two stacked layers of 64 and 32 units, trained with the Adam optimiser, dropout of 0.2, and early stopping on the validation loss.

Staged Residual Correction

A staged residual correction scheme was subsequently developed to determine whether combining complementary machine-learning predictions could improve upon both the individual learners and the mathematical baselines. The first-stage residual was calculated as:

$$\mathbf{e}_k^{(1)} = \mathbf{y}_k - \hat{\mathbf{y}}_k^{(1)} \qquad (15)$$

A second learner was fitted to the residual left by the first stage:

$$\hat{\mathbf{y}}_k^{\mathrm{stg}} = \hat{\mathbf{y}}_k^{(1)} + g(\mathbf{x}_k) \qquad (16)$$

where $\hat{\mathbf{y}}_k^{(1)}$ is the first-stage prediction, $\mathbf{e}_k^{(1)}$ is the residual it leaves, $g(\boldsymbol{x}_k)$ is the residual prediction and $\hat{\mathbf{y}}_k^{\mathrm{stg}}$ is the combined prediction. All stages were trained using the subset only.

The predicted RAC correction was rotated into the ECEF frame and applied to the broadcast satellite position:

$$\mathbf{r}^{\mathrm{corr}} = \mathbf{r}^{\mathrm{bc}} + \mathbf{R}^{\mathsf{T}}\hat{\mathbf{y}}^{\mathrm{stg}}, \qquad (17)$$

where $\mathbf{r}^{\mathrm{corr}}$ is the corrected satellite position and $\mathbf{R}$ is the rotation matrix from ECEF to the RAC frame built from the unit vectors of Equation (4).

Model Evaluation

The models were evaluated using RMSE and MAE, where:

$$\mathrm{RMSE} = \sqrt{\frac{1}{n}\sum_{k=1}^{n}(y_k - \hat{y}_k)^2}, \qquad \mathrm{MAE} = \frac{1}{n}\sum_{k=1}^{n}|y_k - \hat{y}_k| \qquad (18)$$

where n is the number of test records, y_k is the observed orbit error, $\hat{y}_k$ is the predicted value, and $\bar{y}$ is the test-set mean.

Improvement is reported as the percentage reduction in RMSE relative to the uncorrected broadcast error,

ISSN 2278-2540 | DOI: 10.51583/IJLTEMAS | Volume XV, Issue VIII, August 2026

$$\eta_{\mathrm{RMSE}} = \left(1 - \frac{\mathrm{RMSE}_{\mathrm{corrected}}}{\mathrm{RMSE}_{\mathrm{unc}}}\right) \times 100\% \qquad (19)$$

where η_{RMSE} is the percentage reduction, $\mathrm{RMSE}_{\mathrm{unc}}$ is the root mean square 3D orbit error over the test subset before any correction, and $\mathrm{RMSE}_{\mathrm{corrected}}$ is the value achieved by the model under test.

Positioning quality was expressed through

$$\mathrm{CEP} \approx 0.59\,(\sigma_E + \sigma_N), \qquad \mathrm{SEP} \approx 0.51\,(\sigma_E + \sigma_N + \sigma_U), \qquad \mathrm{2DRMS} = 2\sqrt{\sigma_E^2 + \sigma_N^2} \qquad (26)$$

where σ_E, σ_N, and σ_U are the standard deviations of the position residuals in the east, north, and up directions, CEP is the radius containing 50 per cent of horizontal fixes, SEP is its three-dimensional counterpart, and 2DRMS is the radius containing roughly 95 per cent of horizontal fixes.

RESULTS

Table 1 gives the monthly statistics per satellite, and the contrast within this small constellation subset is the first substantive result. The two EGNOS satellites were stable and well behaved. S23 held a mean 3D error of 1.270 to 1.278 m across the three months, and S36 held 1.239 to 1.308 m, with standard deviations between 0.540 and 0.563 m and 95th percentiles below 2.4 m. S27 behaved differently. Its mean sat near 2.6 m in January and February, roughly twice the EGNOS level, and in March its mean fell to 1.196 m while its standard deviation jumped to 3.380 m, driven by a single epoch reaching 97.250 m. That combination, a lower mean with a far larger spread, is the signature of a small number of extreme epochs superimposed on an otherwise ordinary series rather than of a gradual degradation.

Table 1. Monthly GEO broadcast orbit error statistics by satellite, January to March 2026.

Month	Satellite	N	Mean (m)	Std (m)	Min (m)	Max (m)	P95 (m)
Jan	S23 (EGNOS)	2301	1.273	0.560	0.097	3.472	2.281
Jan	S27 (GAGAN)	1923	2.588	2.499	0.055	11.514	7.792
Jan	S36 (EGNOS)	2301	1.308	0.563	0.085	3.744	2.361
Feb	S23 (EGNOS)	2879	1.278	0.558	0.042	3.722	2.283
Feb	S27 (GAGAN)	2761	2.671	2.386	0.052	11.431	7.496
Feb	S36 (EGNOS)	2881	1.267	0.548	0.078	3.416	2.250
Mar	S23 (EGNOS)	1993	1.270	0.550	0.090	3.567	2.269
Mar	S27 (GAGAN)	1781	1.196	3.380	0.052	97.250	2.269
Mar	S36 (EGNOS)	1997	1.239	0.540	0.052	3.548	2.230

Figure 3 supports the satellite-level differences reported in Table 1. Both the drag and polynomial models, which served as the mathematical baselines produced substantially larger errors for S27 than for the two EGNOS satellites. S27 recorded an overall RMSE of approximately 2.7 m and an MAE of 1.6 to 1.7 m, whereas S23 and S36 had RMSE values near 0.6 m and MAE values near 0.45 m. The much larger difference between the RMSE and MAE for S27 indicates that occasional large errors had a strong effect on its RMSE, consistent with the extreme March value of 97.250 m reported in Table 1. The polynomial model produced slightly lower RMSE and MAE values than the drag model for all three satellites, although the improvement

ISSN 2278-2540 | DOI: 10.51583/IJLTEMAS | Volume XV, Issue VIII, August 2026

was modest. Thus, model choice produced a smaller effect than the differences in error behaviour among the satellites.

The machine-learning results extend this comparison by showing clear differences in monthly predictive accuracy. As shown in Figure 4, SVR produced consistently low RMSE values, increasing moderately from 0.148 m in January to 0.200 m in March. Random Forest was similarly stable, with RMSE values between 0.242 and 0.263 m. XGBoost achieved the lowest error in January at 0.107 m, but its performance deteriorated to 0.265 m in February and 0.388 m in March. In contrast, LSTM recorded the highest RMSE in every month, reaching 1.346 m in January and 1.465 m in February before declining to 0.842 m in March. These results indicate that SVR provided the most consistent performance across the study period, while XGBoost produced the best result for an individual month.

Figure 3. Overall RMSE and MAE of the drag and polynomial orbit-error models for EGNOS S23 and S36 and GAGAN S27, January to March 2026.

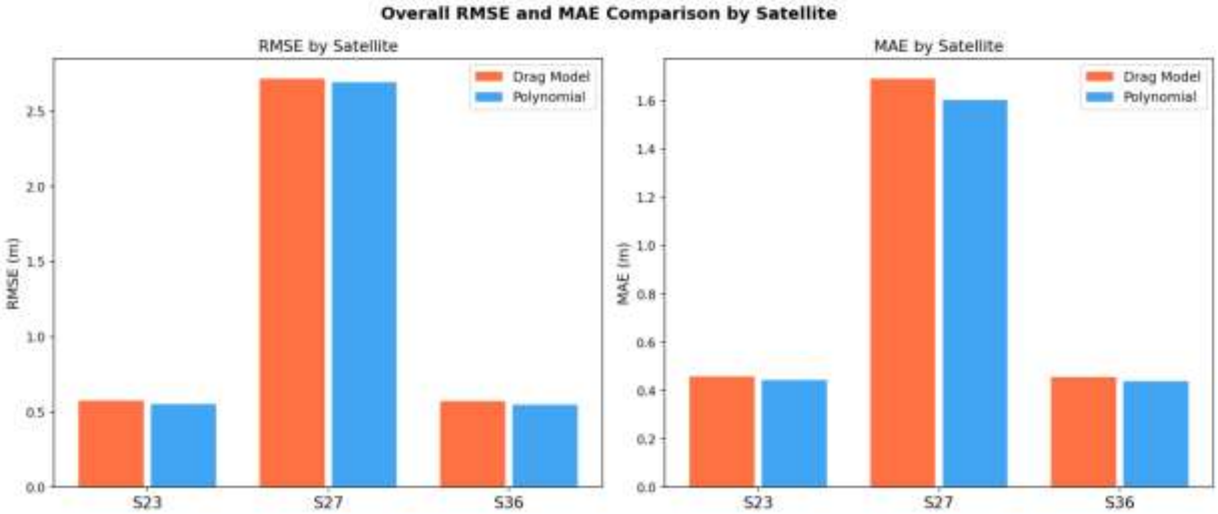

Figure 4. Monthly RMSE comparison of Random Forest, XGBoost, Support Vector Regression and Long Short-Term Memory models, January to March 2026.

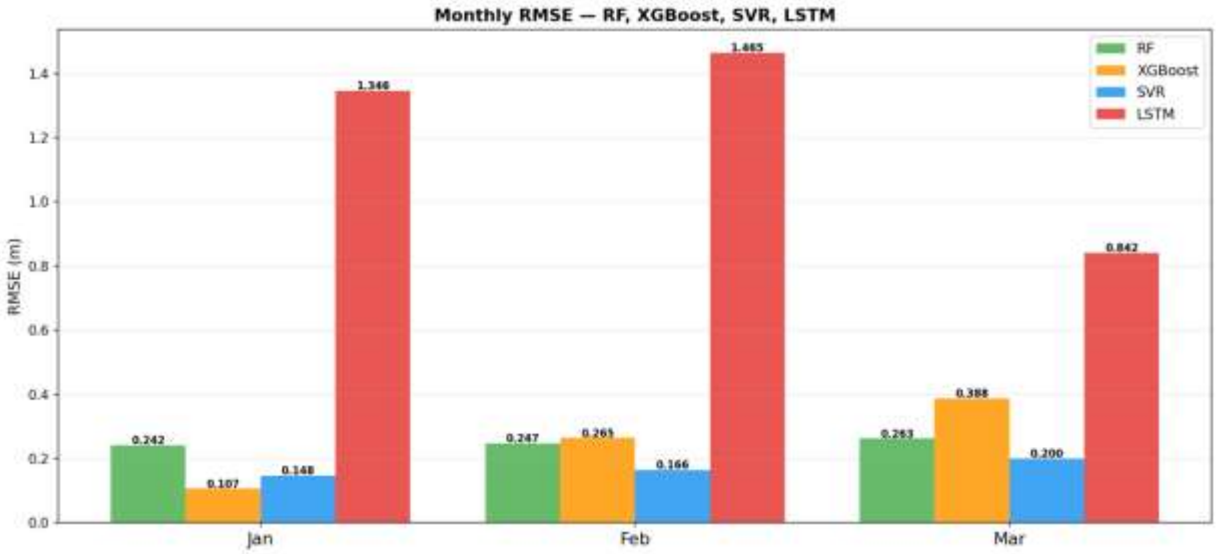

Figure 5 shows that all correction methods improved positioning accuracy relative to the uncorrected solution, although the extent of improvement varied considerably. The uncorrected solution produced the highest errors, with CEP, SEP and 2DRMS values of 2.406 m, 4.117 m and 10.690 m, respectively. The drag and polynomial models reduced these errors, but their performance remained weaker than that of most machine-learning methods. LSTM also produced comparatively high errors of 1.015 m, 1.769 m and 6.428 m.

ISSN 2278-2540 | DOI: 10.51583/IJLTEMAS | Volume XV, Issue VIII, August 2026

XGBoost achieved the lowest CEP and SEP values at 0.375 m and 0.599 m, corresponding to reductions of approximately 84.4% and 85.5% relative to the uncorrected solution. The hybrid model recorded competitive CEP and SEP values of 0.404 m and 0.657 m and produced the lowest 2DRMS value of 1.144 m, representing an improvement of approximately 89.3%. SVR followed closely with a 2DRMS of 1.168 m. These results show that XGBoost performed best for central horizontal and three-dimensional accuracy, while the hybrid model provided the strongest reduction in the broader horizontal-error measure.

Figure 5. Comparison of uncorrected and corrected positioning accuracy using CEP, SEP and 2DRMS for the machine learning and hybrid models.

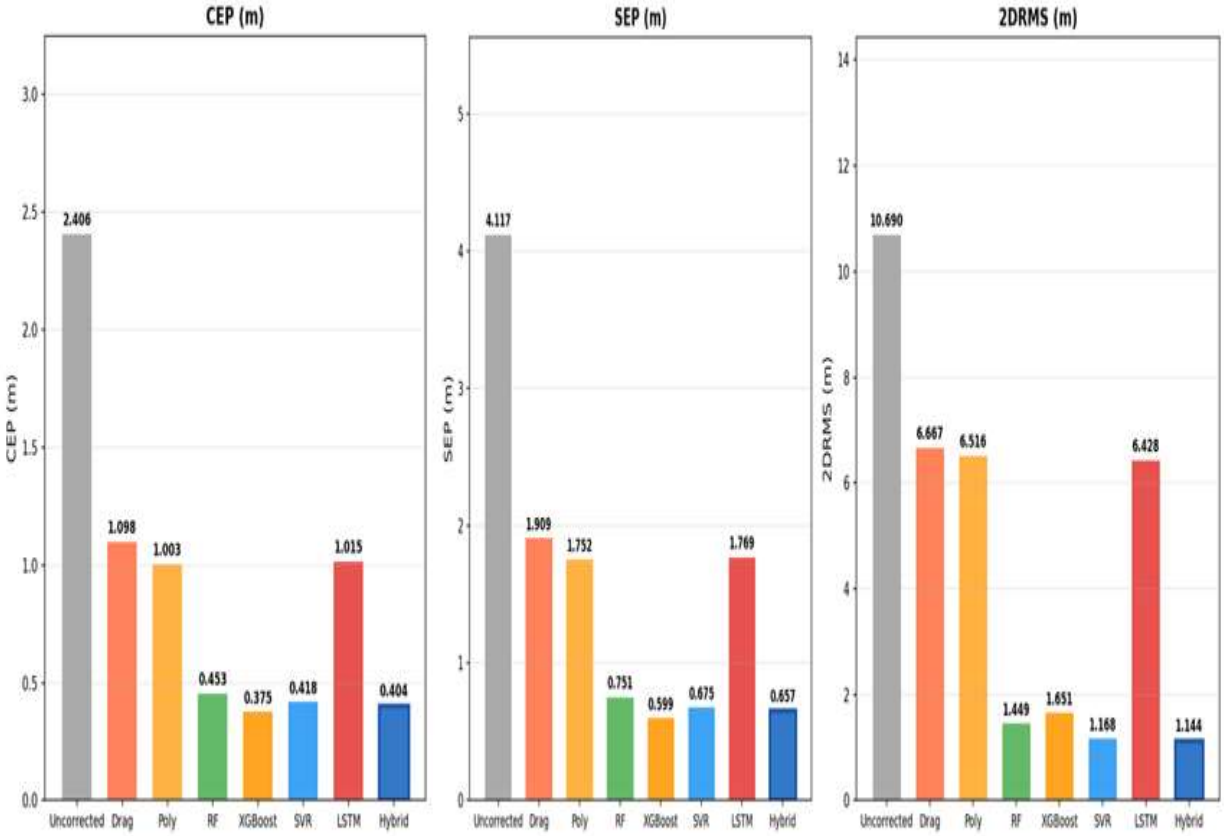

Table 2 quantifies the improvements shown in the hybrid-correction graph using an estimated uncorrected RMSE of 2.278 m. The atmospheric drag and piecewise polynomial models reduced the original error by 41.7% and 43.2%, respectively. LSTM produced a similar reduction of 43.7%, indicating little improvement over the two mathematical models. The tree-based models performed substantially better, with XGBoost and Random Forest reducing RMSE by 88.1% and 89.0%. Support vector regression achieved an RMSE of 0.171 m, corresponding to a 92.5% reduction. The staged hybrid residual scheme recorded the lowest RMSE of 0.164 m and the largest reduction of 92.8%, although its improvement over SVR was only 0.007 m.

Table 2. GEO model comparison and RMSE reduction relative to the uncorrected broadcast orbit error.

Model	RMSE (m)	Reduction (%)
Uncorrected broadcast orbit error	2.278	0.0
Atmospheric drag model	1.329	41.7
Piecewise polynomial model	1.293	43.2
LSTM	1.282	43.7

ISSN 2278-2540 | DOI: 10.51583/IJLTEMAS | Volume XV, Issue VIII, August 2026

XGBoost	0.272	88.1
Random forest	0.250	89.0
Support vector regression	0.171	92.5
Staged hybrid residual scheme	0.164	92.8

Figure 6 shows the temporal change in the GEO 3D orbit error before and after application of the staged hybrid correction. Before correction, the error generally remained between approximately 0.9 and 1.3 m, although it fell below this range on several March dates and rose above 3 m at the end of the observation period. After correction, the error was mostly between 0.06 and 0.13 m, with a pronounced minimum near 0.004 m in mid-February. Although the corrected error increased slightly during late February and early March, it remained consistently below the corresponding uncorrected values throughout the study period. The separation between the two series, shown by the shaded region, confirms that the hybrid combination of Random Forest, XGBoost, SVR and LSTM reduced the error across all evaluated epochs. The resulting RMSE reduction of 92.8% demonstrates that the staged hybrid model removed most of the predictable component of the GEO broadcast orbit error, including periods when the uncorrected error increased sharply.

Figure 6. Temporal comparison of GEO 3D orbit error before and after staged hybrid correction, January to March 2026.

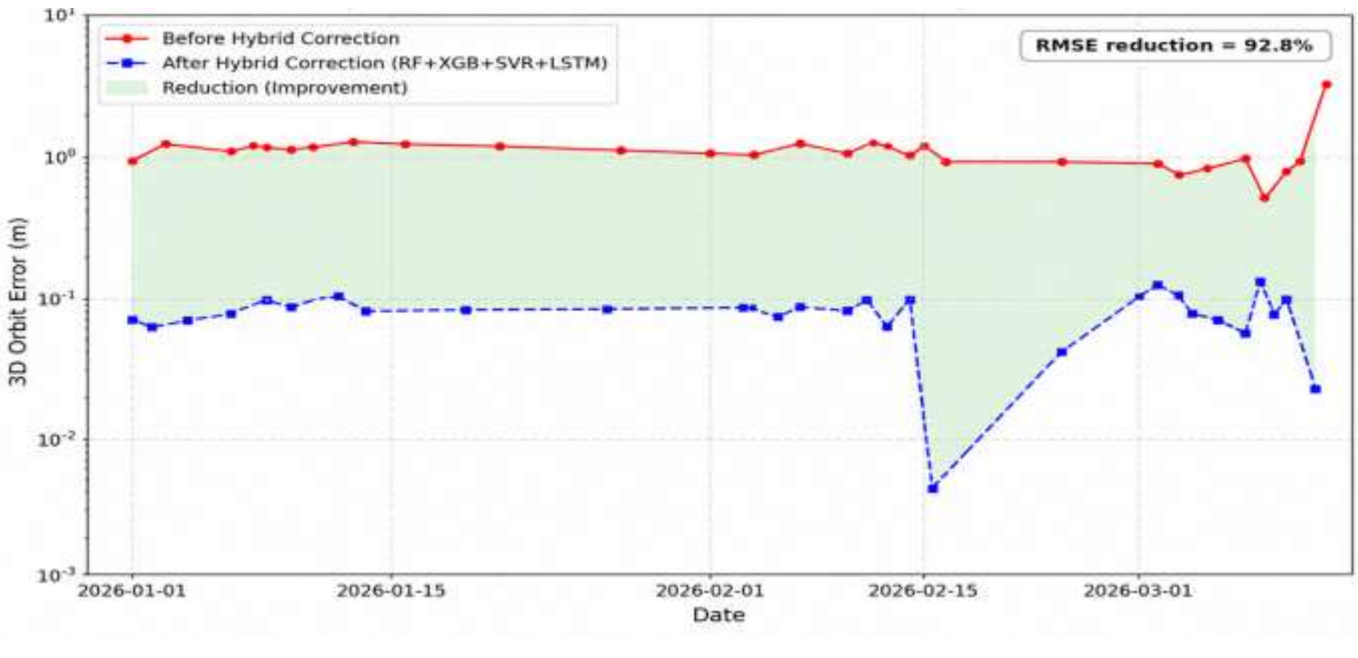

DISCUSSION

The results show clear differences in GEO broadcast orbit-error behaviour among the three satellites. S23 and S36 were stable throughout the observation period, with monthly mean errors between 1.239 and 1.308 m, standard deviations near 0.55 m and 95th-percentile values below 2.4 m. In contrast, S27 recorded mean errors of approximately 2.6 m in January and February. Its March maximum of 97.250 m caused the standard deviation to increase to 3.380 m, although the mean fell to 1.196 m. This pattern indicates isolated extreme epochs rather than continuous deterioration and demonstrates the need for satellite-level screening before GEO observations are used for positioning.

The atmospheric drag and piecewise polynomial models were used as mathematical baselines. They reduced the uncorrected RMSE of approximately 2.278 m to 1.329 and 1.293 m, representing reductions of 41.7% and 43.2%, respectively. Their similar performance confirms that atmospheric drag has little influence at GEO altitude and that a simple polynomial cannot adequately represent abrupt or nonlinear broadcast-error variations. The larger RMSE than MAE recorded for S27 also shows that its baseline results were strongly affected by extreme observations.

The machine-learning models performed considerably better. SVR was the strongest individual model, with an overall RMSE of 0.171 m and a reduction of 92.5%. Random Forest and XGBoost achieved RMSE values of 0.250 and 0.272 m, corresponding to reductions of 89.0% and 88.1%. LSTM was substantially weaker, recording an RMSE of 1.282 m and a reduction of 43.7%, only slightly better than the mathematical baselines. The poor LSTM performance suggests that the available dataset was better suited to conventional machine-learning methods than to a sequence-based neural network.

The staged hybrid residual scheme produced the lowest overall RMSE of 0.164 m and the largest reduction of 92.8%. The temporal comparison shows that the corrected orbit error remained below the uncorrected error throughout the observation period, including epochs with unusually large errors. Its improvement over SVR was small at 0.007 m, but it indicates that a limited amount of predictable structure remained after the first correction stage.

The orbit corrections also improved positioning accuracy. XGBoost produced the lowest CEP and SEP values of 0.375 and 0.599 m, whereas the hybrid model achieved the lowest 2DRMS of 1.144 m. Thus, XGBoost performed best for the central position-error distribution, while the hybrid model provided the strongest control of the wider horizontal-error distribution. These findings confirm that GEO broadcast orbit errors at the Ogbomoso station contained nonlinear and satellite-specific patterns that were better represented by data-driven models than by atmospheric drag or piecewise polynomial baselines.

CONCLUSION

This study found that GEO broadcast orbit errors observed at Ogbomoso varied substantially among satellites, with S23 and S36 remaining stable while S27 contained isolated extreme errors. The atmospheric drag and piecewise polynomial baselines produced limited improvements, whereas the machine-learning models achieved considerably lower errors. The staged hybrid residual scheme performed best, reducing RMSE from approximately 2.278 m to 0.164 m, equivalent to 92.8%. It also produced the lowest 2DRMS of 1.144 m. These findings demonstrate that GEO broadcast orbit errors contain predictable nonlinear patterns that can be corrected effectively using data-driven methods. However, longer observation periods, more satellites and operationally available predictors are required before real-time application.

ACKNOWLEDGEMENTS

The authors thank the Department of Pure and Applied Physics, Ladoke Akintola University of Technology, Ogbomoso, for hosting the LAUTECH GNSS Laboratory, and acknowledge the International GNSS Service and the NASA Crustal Dynamics Data Information System for the precise orbit and clock products, and the NOAA Space Weather Prediction Centre for the space weather indices used in this study.

Data Availability

The RINEX observation and navigation files, the processed GEO orbit error datasets, and the processing scripts, including the direct RINEX 3 SBAS state-vector parser, are available from the corresponding author on reasonable request. IGS Final products are publicly available from the CDDIS archive.

REFERENCES

1. Adewumi, A.S., Àlàgbé, G.A., Azeez, I.A., Ayantunji, G.B., Ogobor, E.A., Oyelowo, O., Fajobi, I. and Eleyele, D.E. (2025). PPP potential of a compact, low-cost GNSS receiver's module in a low latitude region: A case study at the LAUTECH GNSS Laboratory, Nigeria. In Adimula, I. et al. (eds.) Proceedings of the 8th URSI-NG Annual Conference (URSI-NG 2024), pp. 175-180. Atlantis Press.

ISSN 2278-2540 | DOI: 10.51583/IJLTEMAS | Volume XV, Issue VIII, August 2026

2. Hohensinn R, Stauffer R, Glaner MF, Herrera Pinzón ID, Vuadens E, Rossi Y, Clinton J, Rothacher M (2022). Low-cost GNSS and real-time PPP, assessing the precision of the u-blox ZED-F9P for kinematic monitoring applications. Remote Sensing 14, 5100.
3. Mohanty A, Gao G (2024). A survey of machine learning techniques for improving Global Navigation Satellite Systems. EURASIP Journal on Advances in Signal Processing 2024, 73.
4. Nie Z, Zhou P, Liu F, Wang Z, Gao Y (2019). Evaluation of orbit, clock and ionospheric corrections from five currently available SBAS L1 services, methodology and analysis. Remote Sensing 11, 411.
5. Prange L, Beutler G, Dach R, Arnold D, Schaer S, Jäggi A (2020). An empirical solar radiation pressure model for satellites moving in the orbit-normal mode. Advances in Space Research 65, 235–250.
6. Pratiwi N, Herdiwijaya D, Ahmad N, Hidayat T, Ikhsan MI (2025). Effect of solar radiation pressure on a geostationary satellite, comparison with spherical and flat models. Journal of Multidisciplinary Applied Natural Science 5, 1088–1108.
7. Robustelli U, Cutugno M, Pugliano G (2023). Low-cost GNSS and PPP-RTK, investigating the capabilities of the u-blox ZED-F9P module. Sensors 23, 6074.
8. Song J, Liu T, Chen X, Wu Z (2024). Satellite navigation message authentication in GNSS, research on message scheduler for SBAS L1. Sensors 24, 360.
9. Soop EM (1994). Handbook of Geostationary Orbits. Springer Science and Business Media, Dordrecht.
10. Yang C (2021). Innovation and development of BeiDou Navigation Satellite System (BDS) project management mode. Frontiers of Engineering Management 8, 312–320.